Rheologica Acta manuscript No.
(will be inserted by the editor)

Holographic microrheology of polysaccharides from *Streptococcus mutans* biofilms

Fook Chiong Cheong · Simone Duarte · Sang-Hyuk Lee · David G. Grier

Received: date / Accepted: date

Abstract We use three-dimensional holographic particle tracking to perform microrheological measurements of model gelled media, including the polysaccharide pellicle of dental biofilms created by the common cariogenic oral pathogen *Streptococcus mutans*. Nanometer-resolution video-rate holographic tracking of embedded colloidal spheres provides accurate measurements of the gels' complex viscoelastic moduli, including insights into these properties' heterogeneity. When applied to polysaccharides of *S. mutans* biofilms, these techniques promise quantitative microscopic assays for candidate therapeutic agents against cariogenic dental biofilms.

Keywords video holographic microscopy; microrheology; biofilms; polysaccharide gel; *Streptococcus mutans*

1 Introduction

The dental pathogen *Streptococcus mutans* exudes ectoenzymes known as glycosyltransferases that polymerize environmental sugars, mainly sucrose, into a robust polysaccharide gel also known as glucans. Glucans are one of the main components of the extracellular matrix in dental biofilms, providing them with bulk and structural integrity. In addition, glucans enable *S. mutans* and other oral bacteria to adhere to the tooth surface, resulting in the formation and establishment of a cariogenic dental biofilm. The presence of a cariogenic dental biofilm, together with some other specific factors, are implicated in tooth decay, the most prevalent infectious disease in humans. Although disrupting the polyglucan pellicle would greatly reduce the incidence of tooth decay, comparatively little is known regarding the physical properties of these biofilms, including the gel network's viscoelastic properties, the only previous studies having been performed on macroscopic model systems (Vinogradov et al., 2004; Shaw et al., 2004; Desprat et al., 2006; Wloka et al., 2006). Consequently, few quantitative metrics have been available to gauge the efficacy of proposed treatments (Vinogradov et al., 2004; Duarte et al., 2003, 2006; Koo et al., 2003).

As a step toward micromechanical screening for new therapeutic agents, this Article introduces holographic microrheology, which extends particle-tracking microrheology (Mason and Weitz, 1995; Mason et al., 1997; Mason, 2000; Chen et al., 2003) through the use of video holographic microscopy (Sheng et al., 2006; Lee and Grier, 2007; Lee et al., 2007). After first demonstrating the efficacy of holographic microrheology through measurements on standard polyethylene oxide (PEO) samples (Dasgupta et al., 2002), we use it to characterize model extracts of *S. mutans* biofilms. This proof-of-concept demonstration establishes microrheology as a viable tool for studying biofilms' viscoelastic properties and sets the stage for parallel and combinatorial

F. C. Cheong
Department of Physics and Center for Soft Matter Research, New York University, New York, NY 10003
Tel.: +1-212-998-7810
Fax: +1-212-995-4016
E-mail: fcc4@nyu.edu

S. Duarte
Department of Basic Science and Craniofacial Biology, College of Dentistry, New York University, New York, NY 10010

S.-H. Lee
Department of Physics, University of California, Berkeley, CA 94720-7300

D. G. Grier
Department of Physics and Center for Soft Matter Research, New York University, New York, NY 10003

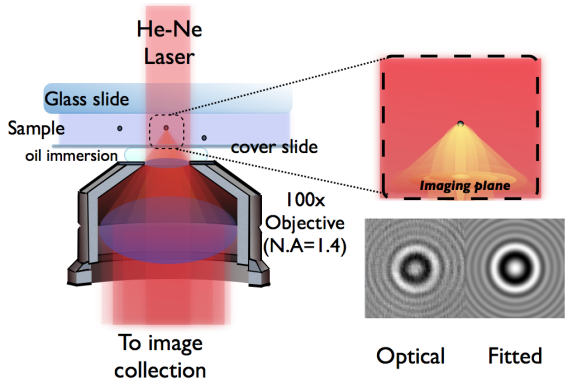

Fig. 1 Principle of holographic particle tracking. Collimated laser light illuminates a sample mounted on an inverted light microscope. Light scattered by a tracer particle interferes with the unscattered portion of the beam in the microscope's focal plane. The magnified hologram then is fit to predictions of Lorenz-Mie theory to obtain the particle's three-dimensional position with nanometer resolution.

studies of biofilms' physical responses to environmental challenges.

2 Holographic microrheology

Microrheology gauges a medium's viscoelastic properties by analyzing its thermally-driven fluctuations, either directly, or through their influence on embedded probe particles. The approach we adopt monitors a probe particle's mean-square fluctuations, $\langle \Delta \boldsymbol{r}^2(t) \rangle$, and uses a generalized Stokes-Einstein relation to extract the medium's frequency-dependent storage modulus, $G'(\omega)$. This is related by the Kramer-Kronig relation to the frequency-dependent loss modulus, $G''(\omega)$, which completes the micromechanical description.

Previous implementations of particle-tracking microrheology have used a variety of particle-tracking techniques including diffusing wave spectroscopy (Pine et al., 1988), dynamic light scattering (Mason and Weitz, 1995; Mason et al., 1997), interferometric particle tracking (Mason and Weitz, 1995; Mason et al., 1997; Gittes et al., 1997), and digital video microscopy (Mason et al., 1997; Meiners and Quake, 1999; Crocker et al., 2000; Chen et al., 2003).

Light scattering approaches provide excellent resolution and bandwidth, but generally yield sample-averaged results, and so are not suitable for inhomogeneous samples. Interferometric methods have similarly high spatial and temporal resolution, and also resolve single-particle trajectories, but can only track one or two particles at a time, and often are limited to in-plane tracking. Conventional particle image velocimetry offers single-particle tracking for many independent probe particles, but at lower spatial and temporal resolution, and typically only for in-plane motions. Many of these issues can be addressed with the introduction of quantitative holographic microscopy (Sheng et al., 2006; Lee and Grier, 2007; Lee et al., 2007), which can track multiple individual particles with nanometer-scale resolution in three dimensions (Lee et al., 2007).

Our holographic microrheology instrument, shown schematically in Fig. 1, consists of a standard inverted optical microscope (Zeiss Axiovert S100 2TV) outfitted with a 100× NA 1.4 oil immersion objective. We implement holographic imaging by replacing the standard bright-field illuminator with a collimated He-Ne laser operating at a vacuum wavelength of $\lambda = 632.8$ nm. Laser light scattered by a probe particle interferes with the unscattered portion of the beam in the focal plane to create an in-line hologram (Sheng et al., 2006; Lee and Grier, 2007). This hologram is magnified by the objective and the 0.63× video eyepiece onto the face of a video camera (NEC TI-324A II) to provide an effective magnification of 101 nm/pixel.

Our probe particles are charge-stabilized polystyrene spheres of nominal radius $a = 0.75$ μm (Duke Scientific, Catalog #5153A, Lot #26621) that are dispersed at random into the sample by vortexing. The sample then is charged into a transparent container formed by bonding a no. 1 glass cover slip to the face of a microscope slide. The sealed sample is allowed to come to thermal and mechanical equilibrium on the microscope stage at $T = 23 \pm 1°\mathrm{C}$.

Holographic images are recorded as an uncompressed digital video stream at 30 frames per second on a digital video recorder (Panasonic DMR-E100H). Each image then is analyzed to measure the probe particle's three-dimensional location relative to the center of the microscope's focal plane.

More specifically, the collimated laser illuminates the probe particle at position $\boldsymbol{r}_p$ with a plane-wave incident electric field, $E_0(\boldsymbol{r}_p) = u_0(\boldsymbol{r}_p)\,\exp(-ikz_p)$, where $k = 2\pi/n_m\lambda$ is the wavenumber of the light in a medium of refractive index n_m. The field scattered by the particle, $E_s(\boldsymbol{r}) = u_0(\boldsymbol{r_p})\, f_m(\boldsymbol{r} - \boldsymbol{r_p})$, propagates to the focal plane at $z = 0$, where it interferes with the incident beam. The distribution of scattered light is described by the Lorenz-Mie scattering function (Bohren and Huffman, 1983), $f_m(\boldsymbol{r} - \boldsymbol{r}_p)$, which depends on the particle's position $\boldsymbol{r}_p$, its radius, a, and its refractive index, n_p.

In practice, the incident illumination varies with position, so that we normalize the measured interference pattern, $I(\boldsymbol{r})$, by a measurement of the incident illumi-

nation $I_0(\boldsymbol{r}) = |u_0(\boldsymbol{r})|^2$ to obtain

$$\frac{I(\boldsymbol{r})}{I_0(\boldsymbol{r})} = 1 + 2\alpha\,\Re\left\{|f_m(\boldsymbol{r}-\boldsymbol{r}_p)|\right\} + \alpha^2\,|f_m(\boldsymbol{r}-\boldsymbol{r}_p)|^2, \quad (1)$$

where $\alpha \approx 1$ accounts for variations in $I_0(\boldsymbol{r_p})$. Equation (1) can be fit to normalized images such as the example in Fig. 1, with the particle's position, radius, and refractive index as free parameters. Whereas conventional bright-field particle tracking on the same instrument offers 10 nm in-plane resolution and 100 nm axial resolution (Crocker and Grier, 1996), holographic particle tracking performs at least one order of magnitude better (Lee et al., 2007). Unlike conventional particle tracking, moreover, holographic tracking does not require separate calibrations for axial measurements.

We assess the measurement error in the particles' positions by tracking probe particles freely diffusing in Newtonian fluids such as water. Provided the particle is far enough from bounding surfaces, its mean-square displacement in each of the three Cartesian directions should evolve according to the Stokes-Einstein relation

$$\left\langle \Delta r_j^2(t) \right\rangle \equiv \langle r_j(t+\tau) - r_j(\tau) \rangle = 2D_0 t, \quad (2)$$

where $D_0 = k_B T/(6\pi\eta a)$ is the diffusion coefficient for a sphere in a fluid of viscosity η at absolute temperature T. The angle brackets in Eq. (2) denote an ensemble average over starting times. Restricting the average to starting times that are separated by the interval t ensures that contributions to $\left\langle \Delta r_j^2(t) \right\rangle$ are statistically independent. When analyzing a single discretely sampled trajectory, however, this choice yields disproportionately large statistical errors at longer lag times, t. Averaging over all starting times improves the estimate for $\left\langle \Delta r_j^2(t) \right\rangle$ and is justified if the trajectory may be treated as a Markov process. This is the case for the thermally driven trajectories we consider, and such exhaustive sampling enables us to estimate the mean-squared displacement from a single trajectory measured over a few thousand time steps. Statistical errors in $\left\langle \Delta r_j^2(t) \right\rangle$ must be corrected for covariances among correlated measurements over the interval t.

Measurements of $r_j(t)$ also suffer from random errors whose mean value, ϵ_j, establishes the tracking resolution. These errors increase the particle's apparent mean-square displacement by $2\epsilon_j^2$ (Crocker and Grier, 1996; Savin and Doyle, 2005), independent of t. A complementary error due to motional blurring during the camera's shutter period, τ_s, reduces the apparent mean-square displacement. The result (Savin and Doyle, 2005),

$$\left\langle \Delta r_j^2(t) \right\rangle = 2D_0 t + 2\left(\epsilon_j^2 - \frac{1}{3} D_0 \tau_s\right) \quad (3)$$

accounts for both effects, and enables us to measure ϵ_j.

The Fourier transform of $\left\langle \Delta r_j^2(t) \right\rangle$ is related to the complex frequency-dependent viscoelastic modulus through the phenomenological generalized Stokes-Einstein relation (Mason et al., 1997; Mason, 2000)

$$G^*(\omega) = -i\,\frac{k_B T}{\pi a \omega\,\left\langle \Delta \tilde{r}_j^2(\omega) \right\rangle} \quad (4)$$

$$\approx i^{\alpha_j(\omega)}\,\frac{k_B T}{\pi a \left\langle \Delta r_j^2(1/\omega) \right\rangle\,\Gamma\left(1+\alpha_j(\omega)\right)}, \quad (5)$$

where $\Gamma(x)$ is the gamma function and

$$\alpha_j(\omega) = \left.\frac{d \ln \left\langle \Delta r_j^2(t) \right\rangle}{d \ln t}\right|_{t=\frac{1}{\omega}}. \quad (6)$$

From this, we obtain

$$G'(\omega) = \Re\{G(\omega)\} \quad \text{and} \quad G''(\omega) = \Im\{G(\omega)\}. \quad (7)$$

$G'(\omega)$ measures the medium's elastic response to shear forces, and $G''(\omega)$ measures its viscosity. They are natural probes of biofilms' responses to potential therapeutic agents. Similarly, the dynamic viscosity,

$$\eta(\omega) = \frac{1}{\omega}\sqrt{G'^2(\omega) + G''^2(\omega)}, \quad (8)$$

provides an overall impression of a biofilm's ability to exchange material with its surroundings.

3 Results

3.1 Newtonian fluid

To establish the accuracy of our holographic microrheology system, we first analyze the motions of a probe particle diffusing in a Newtonian fluid. The five-minute trajectory plotted in Fig. 2 was obtained for a single polystyrene sphere of nominal radius $a = 0.75$ μm suspended in a density matched solution of 25% (w/w) glycerol in water whose viscosity is expected to be 1.7 mPa s. The particle was positioned with an optical tweezer at the midplane of a 50 μm thick sample volume to minimize hydrodynamic coupling to the glass walls (Dufresne et al., 2001) and then was released to acquire data.

Fitting images to the Lorenz-Mie scattering formula yields an estimated single-image precision of $\epsilon_x = \epsilon_y = 4$ nm and $\epsilon_z = 20$ nm (Lee et al., 2007). The mean-square displacement for each coordinate is plotted in Fig. 2 together with a fit to Eq. (3). All three traces are consistent with $D_0 = 0.1695 \pm 0.0001$ μm^2/s. When combined with the trajectory average of the particle's measured radius, $a = 0.775 \pm 0.014$ μm, this suggests an overall viscosity of $\eta = 1.67 \pm 0.01$ mPa s. Given the shutter period of $t_s = 1$ ms, the extrapolated offsets

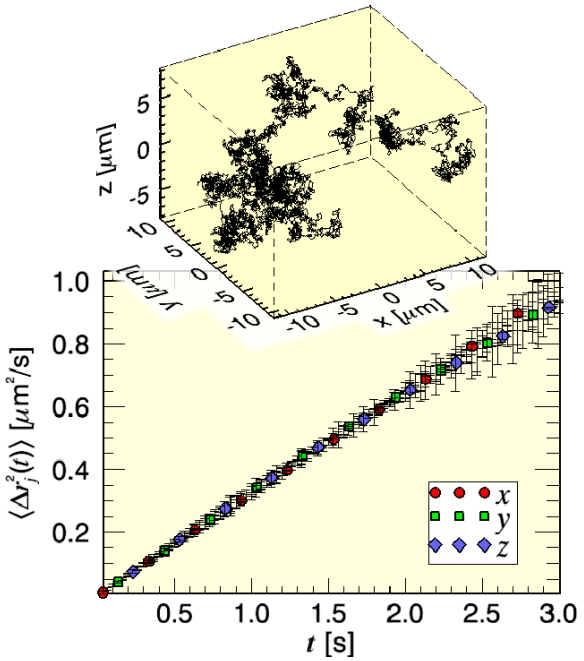

Fig. 2 Measured three-dimensional trajectory of a polystyrene bead freely diffusing in a newtonian fluid. Extrapolating the mean-square displacement of the trajectory to $t = 0$ yields the mean positional measurement error in each cartesian coordinate.

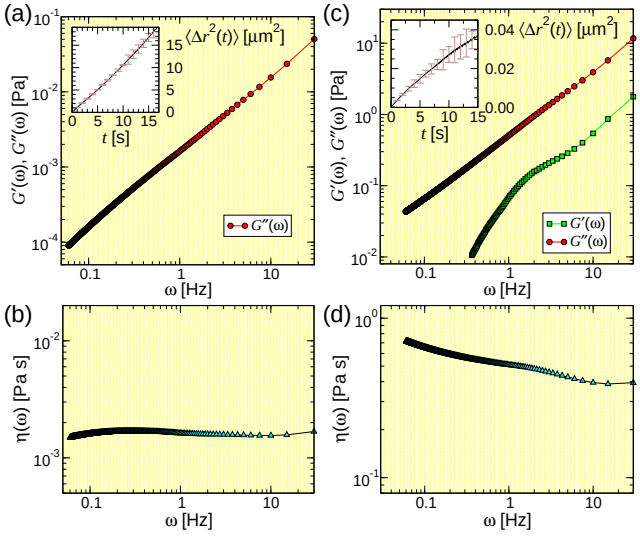

Fig. 3 (a) Viscoelastic moduli, $G'(\omega)$ and $G''(\omega)$, extracted from the data in Fig. 2 for a glycerol-water mixture. (b) The associated dynamic viscosity $\eta(\omega)$. (c) Viscoelastic moduli for a 17 wt % sample of 250 kDa PEO in water. Inset: MSD of the probe particle's trajectory. (d) Dynamic viscosity.

yield $\epsilon_x = \epsilon_y = 8 \pm 4$ nm and $\epsilon_z = 35 \pm 8$ nm. These values are consistent with the estimated single-frame resolution and suggest that the accuracy of the position measurement is comparable to its precision.

The availability of high-resolution axial tracking data is one of the principal benefits of holographic particle tracking for microrheology. Consistency among the three data sets in this case confirms the measurements' freedom from hydrodynamic coupling to the surfaces. More generally such comparisons are useful for gauging a sample's isotropy and homogeneity.

Because results from the three coordinates are in agreement, we analyze the three-dimensional mean-squared displacement, $\langle \Delta r^2(t) \rangle = \sum_{j=1}^{3} \langle \Delta r_j^2(t) \rangle$, with Eqs. (4), (6) and (8) to obtain the loss modulus, $G''(\omega)$, plotted in Fig. 3(a) and the dynamic viscosity, $\eta(\omega)$, plotted in Fig. 3(b). As expected, the glycerol-water solution acts as a Newtonian fluid whose storage modulus, $G'(\omega)$, is too small to resolve over the range of frequencies probed. Its viscosity, $\eta(\omega) = 1.680 \pm 0.001$ mPa s is therefore independent of frequency and agrees with values obtained from bulk measurements.

3.2 Non-Newtonian Fluid

Having established the accuracy of our three-dimensional particle tracking method and the mechanical stability of our instrument, we next demonstrate its efficacy for particle-tracking microrheology by applying it to a standard non-Newtonian sample, an aqueous solution of high-molecular-weight PEO. Figure 3(c) shows $G'(\omega)$ and $G''(\omega)$ obtained from a single sphere dispersed in a 17 wt % solution of 200 kDa PEO in deionized water. As for the Newtonian fluid, consistent results are obtained in all three coordinates, so that combined results are presented in Figs. 3(c) and (d).

The viscoelastic moduli, plotted in Fig. 3(c), agree quantitatively with results reported for similar samples under comparable conditions (Dasgupta et al., 2002). The loss modulus, $G''(\omega)$, exceeds the storage modulus, $G'(\omega)$, over the entire frequency range, which identifies this sample as a fluid, rather than a gel. The associated dynamic viscosity, plotted in Fig. 3(d), decreases monotonically with increasing frequency, which is the signature of a shear-thinning fluid.

3.3 *S. mutans* biofilm

The data in Fig. 4 show comparable results for biofilm polysaccharides. Pioneering studies of biofilm's structure (Lawrence et al., 1991; Costerton et al., 1995) have revealed a degree of heterogeneity at the sub-millimeter scale that might seem unamenable to systematic physical analysis. Indeed, measurements of model biofilms' macroscopic rheological properties (Stoodley et al., 1999; Korstgens et al., 2001; Klapper et al., 2002; Towler et al., 2003; Shaw et al., 2004; Vinogradov et al., 2004;

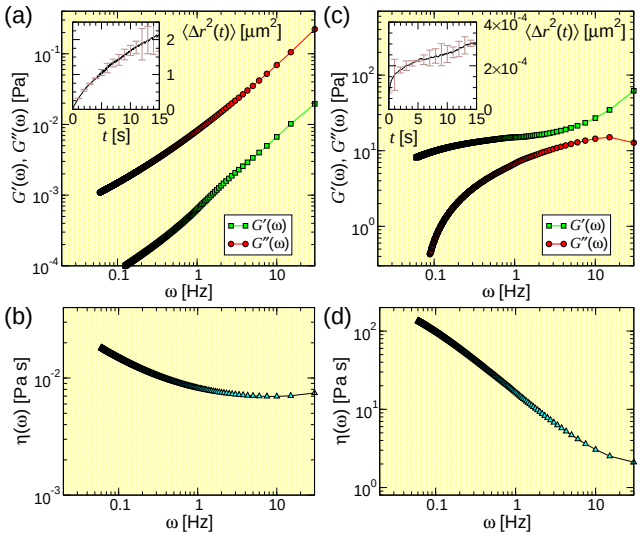

Fig. 4 (a) Viscoelastic moduli, $G'(\omega)$ and $G''(\omega)$, of a reconstituted S-type polysaccharide biofilm. The MSD of the probe particle is inset. (b) Dynamic viscosity of the S-type biofilm. (c) and (d) show the corresponding results for the N-type polysaccharide at the same concentration.

Cense et al., 2006) have yielded viscoelastic moduli differing by more than three orders of magnitude, even for nominally similar samples. These differences have been attributed to loading, strain rate, total strain and sample preparation (Cense et al., 2006).

Microrheology addresses many of these concerns by probing the local-scale properties of unloaded samples in equilibrium. Although particle-tracking microrheology has been applied to a wide range of industrially and biologically relevant materials, its application to biofilms appears to be novel. Model biofilms can be prepared without the complication of swimming bacteria, and so lend themselves to this kind of analysis.

Streptococcus mutans polysaccharide samples were extracted from 5-day-old biofilms of *S. mutans* UA159 (ATCC 700610) that were grown on glass slides in the presence of 10% sucrose (Koo et al., 2003). Water-soluble (S) polysaccharides were extracted with MilliQ water at room temperature. The insoluble (N) polysaccharide fraction then was extracted in 1N NaOH. Both extracts were neutralized to pH 7.0 ± 0.5 and precipitated with cold ethanol (75% v/v) at $-18°$C for at least 24 h. The resulting polysaccharide samples have a mean molecular weight of about 10 kDa with a polydispersity of at least 50 percent, and contain trace amounts of protein (Cury et al., 2000). After precipitation, the samples were washed several times with 75% (v/v) ethanol, blot-dried and and dissolved in water (S) or 1N NaOH (N), at 20% (w/v) to form the gels used in the microrheological measurements. Polystyrene probe particles were dispersed at random in the polysaccharide at this time, and particles near the mid-plane of the sealed sample chamber were selected for measurement.

Results for the S fraction, plotted in Figs. 4(a) and (b), resemble those for the PEO solution in Figs. 3(c) and (d). The biofilm's water-soluble polysaccharides form a shear-thinning fluid roughly ten times more viscous than water.

The data in Fig. 4(c), by contrast, show that the N-type fraction forms an elastic gel with a typical storage modulus of 10 Pa. This is several hundred times smaller than the mean value reported for bulk samples of *S. mutans* polysaccharides in Ref. (Vinogradov et al., 2004). It is consistent, however, with values reported at the lowest loadings when the substantial measurement error is taken into account (Vinogradov et al., 2004). Accurate measurements at low loading are one of the strengths of microrheology, so that the results in Figs. 4(c) and (d) are more likely to reflect the biofilm's properties *in vivo*. Even at low loading, the N-type gel is strongly shear-thinning, as indicated by its dynamic viscosity in Fig. 4(d). This is a desirable trait for dental biofilms because it facilitates removal by brushing.

These observations suggest complementary roles of the two fractions in establishing the biofilm's mechanical and biological properties *in vivo*. The N-type material appears better suited to play the role of the mechanical scaffold within which the biofilm's bacterial colony establishes its ecosystem. Ability to disrupt the N-type gel, therefore, might be considered a promising characteristic for therapeutic agents. Microrheological assays of such agents' influence on N-type extracts should provide a simple and cost-effective screening technique. The ability of holographic microrheology to track multiple probe particles simultaneously furthermore creates opportunities for screening multiple therapeutic agents individually and in combination as a function of concentration.

4 Discussion

We have demonstrated that precise measurements of probe particles' three-dimensional trajectories made possible by video holographic microscopy lend themselves naturally to applications in particle-imaging microrheology. Applying this technique to biofilms, in particular, shows promise for high-throughput combinatorial screening of candidate therapeutic or remedial agents. Rather than assessing their biological or biochemical influence, holographic microrheology offers direct insight into these agents' influence on biofilms' physical properties. In the case of dental biofilms, the availability of model polysaccharide gels will greatly simplify the development of standard assays for therapeutic

agents. Because microrheological measurements require only micrometer-scale samples, very large arrays of independent assays should be possible in centimeter-scale systems, with each assay requiring just a few minutes of holographic recording.

5 Acknowledgments

This work was supported by the National Science Foundation under Grant Number DMR-0606415.

References

Bohren CF, Huffman DR (1983) Absorption and Scattering of Light by Small Particles. Wiley Interscience, New York

Cense AW, Peeters EAG, Gottenbos B, Baaijens FPT, Nuijs AM, van Dongen MEH (2006) Mechanical properties and failure of *Streptococcus mutans* biofilms, studied using a microindentation device. J Microbio Methods 67:463–472

Chen DT, Weeks ER, Crocker JC, Islam MF, Verma R, Gruber J, Levine AJ, Lubensky TC, Yodh AG (2003) Rheological microscopy: Local mechanical properties from microrheology. Phys Rev Lett 90:108301

Costerton JW, Lewandowski Z, Caldwell DE, Korber DR, Lappin-Scott HM (1995) Microbial biofilms. Annu Rev Microbiol 49:711–745

Crocker JC, Grier DG (1996) Methods of digital video microscopy for colloidal studies. J Colloid Interface Sci 179:298–310

Crocker JC, Valentine MT, Weeks ER, Gisler T, Kaplan PD, Yodh AG, Weitz DA (2000) Two-point microrheology of inhomogeneous soft materials. Phys Rev Lett 85:888–891

Cury JA, Rebelo MA, Del Bel Cury AA, Derbyshire MT, Tabchoury CP (2000) Biochemical composition and cariogenicity of dental plaque formed in the presence of sucrose or glucose and fructose. Caries Res 34:491–497

Dasgupta BR, Tee SY, Crocker JC, Frisken BJ, Weitz DA (2002) Microrheology of polyethylene oxide using diffusing wave spectroscopy and single scattering. Phys Rev E 65:051505

Desprat N, Guiroy A, Asnacios A (2006) Microplates-based rheometer for a single living cell. Rev Sci Instrum 77:055111

Duarte S, Gregoire S, Singh AP, Vorsa N, Schaich K, Bowen WH, Koo H (2006) Inhibitory effects of cranberry polyphenols on formation and acidogenicity of *Streptococcus mutans* biofilms. FEMS Microbiol Lett 257:50–56

Duarte S, Koo H, Bowen WH, Hayacibara MF, Cury JA, Ikegaki M, Rosalen PL (2003) Effect of a novel type of propolis and its chemical fractions on glucsyltransferases and on growth and adherence of mutans streptococci. Biol Pharm Bull 26:527–531

Dufresne ER, Altman D, Grier DG (2001) Brownian dynamics of a sphere in a slit pore. Europhys Lett 53:264–270

Gittes F, Schnurr B, Olmsted PD, MacKintosh FC, Schmidt CF (1997) Microscopic viscoelasticity: Shear moduli of soft materials determined from thermal fluctuations. Phys Rev Lett 79:3286–3289

Mason TG, Dhople A, Wirtz D (1997) Concentrated DNA rheology and microrheology. In: MRS Proceedings on Statistical Mechanics ¿ in Physics and Biology 463:153–158

Klapper I, Rupp CJ, Cargo R, Purvedorj B, Stoodley P (2002) Viscoelastic fluid description of bacterial biofilm material properties. Biotech and Bioeng 80:289–296

Koo H, Hayacibara MF, Cury BD, Rosalen PL, Park YK, Vacca-Smith AM, Bowen WH (2003) Inhibition of *Streptococcus mutans* biofilm accumulation and polysaccharide production by apigenin and tt-farnesol. J Antimicrob Chemother 52:782–789

Korstgens V, Flemming HC, Wingender J, Borchard W (2001) Uniaxial compression measurement device for investigation of the mechanical stability of biofilms. J Microbiol Methods 46:9–17

Lawrence JR, Korber DR, Hoyle BD, Costerton JW, Caldwell DE (1991) Optical sectioning of microbial biofilms. J Bacteriol 173:6558–6567

Lee SH, Grier DG (2007) Holographic microscopy of holographically trapped three-dimensional structures. Opt Express 15:1505–1512

Lee SH, Roichman Y, Yi GR, Kim SH, Yang SM, van Blaaderen A, van Oostrum P, Grier DG (2007) Characterizing and tracking single colloidal particles with video holographic microscopy. Opt Express 15:18275–18282

Mason TG (2000) Estimating the viscoelastic moduli of complex fluids using the generalized stokes-einstein equation. Rheologica Acta 39:371–378

Mason TG, Ganesan K, van Zanten JH, Wirtz D, Kuo SC (1997) Particle tracking microrheology of complex fluids. Phys Rev Lett 79:3282–3285

Mason TG, Weitz DA (1995) Optical measurements of frequency-dependent viscoelastic moduli of complex fluids. Phys Rev Lett 74:1250–1253

Meiners JC, Quake SR (1999) Direct measurement of hydrodynamic cross correlations between two particles in an external potential. Phys Rev Lett 82:2211–2214.

Pine DJ, Weitz DA, Chaikin PM, Herbolzheimer E (1988) Diffusing wave spectroscopy. Phys Rev Lett 60:1134–1137

Savin T, Doyle PS (2005) Static and dynamic errors in particle tracking microrheology. Biophys J 88:623–638

Shaw T, Winston M, Rupp CJ, Klapper I, Stoodley P (2004) Commonality of elastic relaxation times in biofilms. Phys Rev Lett 93:098102

Sheng J, Malkiel E, Katz J (2006) Digital holographic microscope for measuring three-dimensional particle distributions and motions. Appl Opt 45:3893–3901

Stoodley P, Lewandowski Z, Boyle JD, Lappin-Scott HM (1999) Structural deformation of bacterial biofilms caused by short-term fluctuations in fluid shear: An in situ investigation of biofilm rheology. Biotech and Bioeng 65:83–92

Towler BW, Rupp CJ, Cunningham AB, Stoodley P (2003) Viscoelastic properties of a mixed culture biofilm from rheometer creep analysis. Biofouling 19:279–285

Vinogradov AM, Winston M, Rupp CJ, Stoodley P (2004) Rheology of biofilms formed from the dental plaque pathogen *Streptococcus mutans*. Biofilms 1:49–56

Wloka M, Rehage H, Flemming HC, Wingender J (2006) Structure and rheological behavior of the extracellular polymeric substance network of mucoid *Pseudomonas aeruginosa* biofilms. Biofilms 2:275–283